Nanoscale

Protein Coating Composition Targets Nanoparticles to Leaf Stomata and Trichomes

Journal:	*Nanoscale*
Manuscript ID	NR-COM-09-2019-008100.R1
Article Type:	Communication
Date Submitted by the Author:	28-Nov-2019
Complete List of Authors:	Spielman-Sun, Eleanor; Carnegie Mellon University, Department of Civil and Environmental Engineering Avellan, Astrid; Carnegie Mellon University, Department of Civil and Environmental Engineering; Center for Environmental Implications of Nanotechnology, Bland, Garret; Carnegie Mellon University, Department of Civil and Environmental Engineering Clement, Emma; Carnegie Mellon University, Department of Civil and Environmental Engineering Tappero, Ryan; Brookhaven National Laboratory, National Synchrotron Light Source II Acerbo, Alvin; University of Chicago Lowry, Gregory; Carnegie Mellon University, Civil and Environmental Engineering; Center for Environmental Implications of Nanotechnology,

Protein Coating Composition Targets Nanoparticles to Leaf Stomata and Trichomes

Eleanor Spielman-Sun[†], Astrid Avellan[†], Garret D. Bland[†], Emma T. Clement[†], Ryan V. Tappero,[‡] Alvin S. Acerbo,[‡,§] Gregory V. Lowry*[†]

[†]Civil and Environmental Engineering, Carnegie Mellon University, Pittsburgh, Pennsylvania 15213, United States

[‡] National Synchrotron Light Source II, Brookhaven National Laboratory, Upton, NY 11973, United States

[§] Center for Advanced Radiation Sources, University of Chicago, Chicago, IL 60637, United States

*Corresponding author:

Address: Carnegie Mellon University, Pittsburgh, PA 15213

Phone: (412) 268-2948

Email: glowry@cmu.edu

KEYWORDS:

Plant nanobiotechnology; pesticides; targeted-delivery; sustainable agriculture

ABSTRACT

Plant nanobiotechnology has the potential to revolutionize agriculture. However, the lack of effective methods to deliver nanoparticles (NPs) to the precise locations in plants where they are needed impedes these technological innovations. Here, model gold nanoparticles (AuNP) were coated with citrate, bovine serum albumin (BSA) as a protein control, or LM6-M, an antibody with an affinity for functional groups unique to stomata on leaf surfaces to deliver the AuNPs to stomata. One-month-old *Vicia fava* leaves were exposed via drop deposition to aqueous suspensions of LM6-M-coated AuNPs and allowed to air dry. After rinsing, Au distribution on the leaf surface was investigated by enhanced dark-field microscopy and x-ray fluorescence mapping. While citrate-coated AuNPs randomly covered the plant leaves, LM6-M-AuNPs strongly adhered to the stomata and remained on the leaf surface after rinsing, and BSA-AuNPs specifically targeted trichome hairs. To the authors' knowledge, this is the first report of active targeting of live leaf structures using NPs coated with molecular recognition molecules. This proof-of-concept study provides a strategy for future targeted nanopesticide delivery research.

INTRODUCTION

By 2050, the global population is projected to be ~9.6 billion and associated global food demand to increase by 70%.[1] The protection of crops against plant disease has an undeniable role to play in meeting the growing demand for food. Plant pathogens reduce agricultural productivity by 20-40%, resulting in billions of dollars of annual losses.[2,3] Globally, ~4 million tons of pesticides are applied each year,[4] and as much as 99% of these applied pesticides do not reach their final target and are wasted.[5] Thus, there is a critical need for innovative disease management solutions to improve the resiliency of U.S. agriculture.[6]

Nanotechnology has the potential to vastly improve crop disease management. Nanomaterials such as nanoparticles (NP) possess unique chemical and physical properties that can be leveraged for better disease management.[7,8] NPs can be synthesized with sizes small enough to enter leaves and transport in phloem.[9,10] There is mounting evidence of foliar application of NPs resulting in successful management of plant diseases.[11,12] Finally, it has been demonstrated that designing NPs surface chemistry allows tuning NP-leaves interactions and uptake.[10,13]

The ability to design NP surface properties has led to significant developments in the use of surface-functionalized nanoparticles as nanocarriers for targeted delivery in medical and biological research. A growing number of studies have demonstrated that “active targeting” of nanoscale drug carriers conjugated with cell-specific targeting ligands (e.g. antibodies, aptamers, peptides) can increase drug delivery to the desired site while decreasing unwanted delivery elsewhere.[14,15] Recently, there has also been some interest in the use of NPs as delivery vehicles

into plants, though most have an emphasis on tuning coating to improve plant uptake.[e.g.10,16–18] Examples of organelle-specific targeting in live plants are generally limited to chloroplasts.[19–21]

Pathogen entry into host tissue is a critical first step leading to infection. Many plant pathogens are known to enter plants through natural openings (e.g. stomata, trichomes, hydathodes) or artificial openings (e.g. points of injury).[22–24] While spraying uncoated NPs onto leaf surfaces results in a random distribution of NPs with low affinity to any particular leaf structure, targeting antimicrobial NPs directly to these disease entry points (e.g. stomatal guard cells, trichomes; **Fig. 1**) can increase the probability of contact between the pathogen and NP. This can potentially increase the efficacy of the pesticide at lower applied rates.

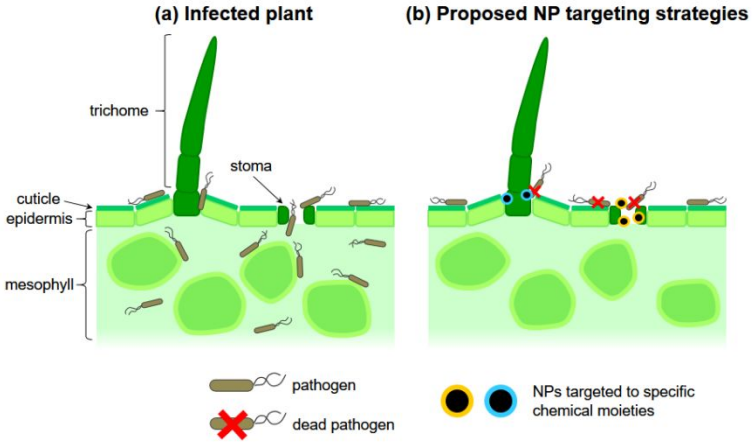

Fig. 1 (**A**) Pathogens on a leaf surface can penetrate open stoma and trichomes, colonizing the apoplast and spreading to other parts of the plant. (**B**) NPs can potentially be targeted directly to specific guard cell wall or trichome-based chemical moieties to efficiently prevent pathogen entry.

Plant leaves are covered with a lipophilic waxy layer (cuticle) 0.1-10 μm thick,[25] but this layer can be thinner at the base of trichomes[26] and on the surface of guard cells and is absent on the stomatal opening.[27] Though the exact chemical composition of guard cells varies between plant species, plant cell walls are generally pectin-rich.[28–30] Using FTIR, Jones et al. identified that guard cells of *Vicia faba* are enriched in phenolic esters of pectin compared to the

surrounding epidermal cells, which had a higher unesterified pectin content.[31] In particular, they identified arabinose sugar content in the stomata as being particularly high. Recently, Cornuault et al. have designed a monoclonal antibody with high avidity to pectic α-1,5-arabinan,[32] which have been fluorescently tagged to image stomatal guard cell walls in fixed tissue.[33,34] Similarly to how monoclonal antibodies have been used as targeting ligands in medicine, we hypothesize that these antibodies coated onto a NP surface could provide targeted affinity to stomata on live plants.

Overall, the goal of this study was to demonstrate targeted delivery of NPs to stomata onto live plants. Gold nanoparticles were coated with either LM6-M, a biomolecule with affinity for α-1,5-arabinan (a chemical moiety found on stomatal guard cells) or bovine serum albumin (BSA) as a model protein standard chosen for it high stability and amphiphilicity,[35,36] but without specific affinity for stomata. *V. faba* leaves were exposed via drop deposition, and NP distribution was evaluated using darkfield imaging and synchrotron X-ray fluorescence mapping (XFM) on fresh plant tissue. To the authors' knowledge, this is the first reported active targeting of NPs onto live plants by coating NPs with molecular recognition molecules.

MATERIALS AND METHODS

Materials: Citrate-reduced AuNPs were synthesized by the Center for the Environmental Implications of Nanotechnology (CEINT) using established methods [37]. AuNPs were chosen as a model NP for the absence of Au background in plant tissue and the ease of coating its metallic surface. Anti-pectic polysaccharide (α-1,5-arabinan) antibody (LM6-M) was purchased from Kerafast (Boston, MA); details regarding isolation and characterization of this rat IgM

monoclonal antibody can be found in Cornuault et al.[32] Bovine Serum Albumin (BSA), a model protein, was purchased from Sigma-Aldrich (St. Louis, MO).

Coating Attachment Protocol: The LM6-M antibody and BSA protein were attached to the AuNP via physisorption.[38,39] The antibody solution was combined with cit-AuNP solution (200 mg/L) in a 1:1 (v/v) ratio, and the BSA solution in a 5:1 (v/v) ratio [35]. Both solutions were mixed in the dark for 48 h before being centrifuged at 10,000 rpm (11,000 x *g*) for 20 min, supernatant decanted, and resuspended in DI water twice to remove excess protein/antibody (method adapted from Oliveira et al[40]). Exposure solutions had a final Au concentration of ~100 mg-Au/L. pH of the final solution was circumneutral.

Nanoparticle Characterization: All AuNP characterization was performed in the exposure solution. Electrophoretic mobility and number-weighted hydrodynamic diameter was measured using a Nano Zetasizer (Malvern Instruments, Westborough, MA). UV-Vis spectra were measured using Cary Series UV-Vis-NIR spectrophotometer (Agilent, Santa Clara, CA). The primary particle size distribution was characterized by transmission electron microscopy (TEM; JEOL JEM-2000EX operating at 200 keV).

Plant Growth and Exposure: Broad bean (*Vicia faba* cv. Windsor) seeds were obtained from Jonny's Selected Seeds (Winslow, ME). *V. faba* was chosen because it is a commonly used model plant in stomatal studies and therefore is well characterized. Seeds were surface sterilized with 10% (w/v) bleach (VWR Analytical) for 10 minutes and then thoroughly rinsed with DI water three times. Seeds were germinated in a DI-water moistened paper towel and germinated in the dark for 10 days. The seedlings were then planted in glass beakers with silica sand (50-70 mesh; Sigma-Aldrich) that was acid-washed, rinsed with DI-water, burned overnight at 500 °C to

remove organics, and rinsed with DI-water again. Plants were grown in a controlled environment chamber (Binder™ Model KBWF 729; day/night photoperiod 16h/8h, day/night temperature 25 °C /21 °C and 60% humidity) for 3 weeks and were watered as needed with ¼ strength Hoagland's nutrient solution. 5 µL of NP solution was dropped on the adaxial side of the plant leaf and allowed to air dry on the bench-top for 4 h. The exposed leaf was then cut-off and rinsed in a 50 mL centrifuge tube filled with a 1 mM $CaCl_2$ basal salt solution under gentle agitation for 2 minutes to remove loosely adhered NPs prior to further analysis.

Microscopy Imaging: The NP distribution on the leaves were visualized using an enhanced darkfield microscope (BX51, Olympus, USA) equipped with a 150 W halogen light source for the darkfield sample illumination (Fiber-Lite®, Dolan-Jenner, USA). The leaves were mounted between a glass slide and a glass coverslips with deionized water and observed with 60× magnification. Images were acquired using 60% light source intensity and 0.5 s acquisition time per line.

X-Ray Fluorescence Imaging: After exposure, fresh plant leaves were placed between Kapton® tape and a piece of 4 µm-thick Ultralene®, which formed a seal around the plant tissue to minimize dehydration. Prior to XFM, microscope images of the drop deposition zone were taken using a Nikon eclipse LVDIA-N in transmission bright field mode. µ-XRF maps were acquired at National Synchrotron Light Source (NSLS-II) at Brookhaven National Laboratory on XFM (4-BM). Samples were oriented at 45° to the incoming microbeam and at 45° to a four-element Vortex-ME4 silicon-drift detector. Large area (> 1 mm) maps with an incident energy of 14.5 keV were created using a step size of 5 µm and a dwell time of 100 ms for LM6M-AuNP exposure, step size of 7 µm and a dwell time of 500 ms for BSA-AuNP exposure, and a step size of 5 µm and a dwell time of 350 ms for the cit-AuNP exposure. Using GSE XRM MapViewer in

Larch (v 0.9.40) [41], K elemental maps (to highlight stomata and trichome structures) were obtained by displaying the K Kα fluorescence peak (3.3 keV), and Au elemental maps (to track AuNPs signal) by using the Au Lβ fluorescence peak (11.4 keV) rather than the Au Lα (9.7 keV), which overlaps with Zn Kβ (9.6 keV).

RESULTS

Materials Characterization: The TEM images of the starting citrate-AuNPs and the coated LM6M- and BSA-AuNPs are shown in **Fig. S1**. A heterogeneous organic coating ~3-5 nm thick on the LM6M-AuNP (**Fig. S1 B-C**) and ~2 nm thick on the BSA-AuNPs (**Fig. S1 D-E**) is visible around the coated particles. Additional particle characteristics are presented in **Table 1**. The primary particle diameter remained similar after being coated. The increase in number-weighted hydrodynamic diameter and λ_{max} shift in the UV-Vis spectra (**Fig. S1 F**) for the BSA-AuNP and LM6M-AuNP confirm the presence of the coating. Between the cit-AuNP and LM6M-AuNP, there is a slight decrease in electrophoretic mobility (and calculated zeta potential), but this difference is not statistically significant. The BSA treatment, however, results in a significant increase in electronegativity. This lower electrophoretic mobility (and therefore zeta potential) is consistent with the adsorption of a macromolecule like the BSA or LM6-M.[42,43]

Table 1: Summary of cit-AuNP, LM6M-AuNP, and BSA-AuNP exposure solution characterization. AuNP concentration was 100 mg/L.

Sample	TEM Diameter (nm)	Hydrodynamic diameter* (nm)	Electrophoretic mobility ($\mu m \cdot cm \cdot V^{-1} \cdot s^{-1}$)	Apparent Zeta Potential (mV)	UV-Vis λ_{max} (nm)
cit-AuNP	12.6 ± 1.0	25.8 ± 7.6	−2.77 ± 0.38	−35.5 ± 4.9	519
LM6M-AuNP	11.6 ± 1.2	81.2 ± 25.4	−2.42 ± 0.43	−31.0 ± 5.5	531
BSA-AuNP	14.0 ± 1.0	18.1 ± 5.3	−4.69 ± 0.39	−60.1 ± 5.0	526

*Number-weighted. Volume-weighted and Z-average hydrodynamic diameters can be found in **Table S1**.

Microscope Detection of AuNPs on Leaf Surface: Light microscope images of control *V. faba* leaves are shown in **Fig. S2**. Stomata, which are indicated with red arrows, were identified by their distinct, "kidney-bean" shaped cells. Enhanced darkfield microscopy images of *V. faba* leaves exposed to LM6M-AuNP, cit-AuNP, BSA-AuNP, or DI water (as a control) are shown in **Fig. 2**. The LM6M-AuNP treatment clearly resulted in accumulation of particles only around the stomata while the cit-AuNP treatment resulted in accumulation over the entire leaf surface. The BSA-AuNP induced no clear association of NPs with the stomata, but showed a high association with the head of glandular trichomes (dark area to the right of the stomata). This trichome association, which is further illustrated in **Fig. S3**, is discussed in greater detail later.

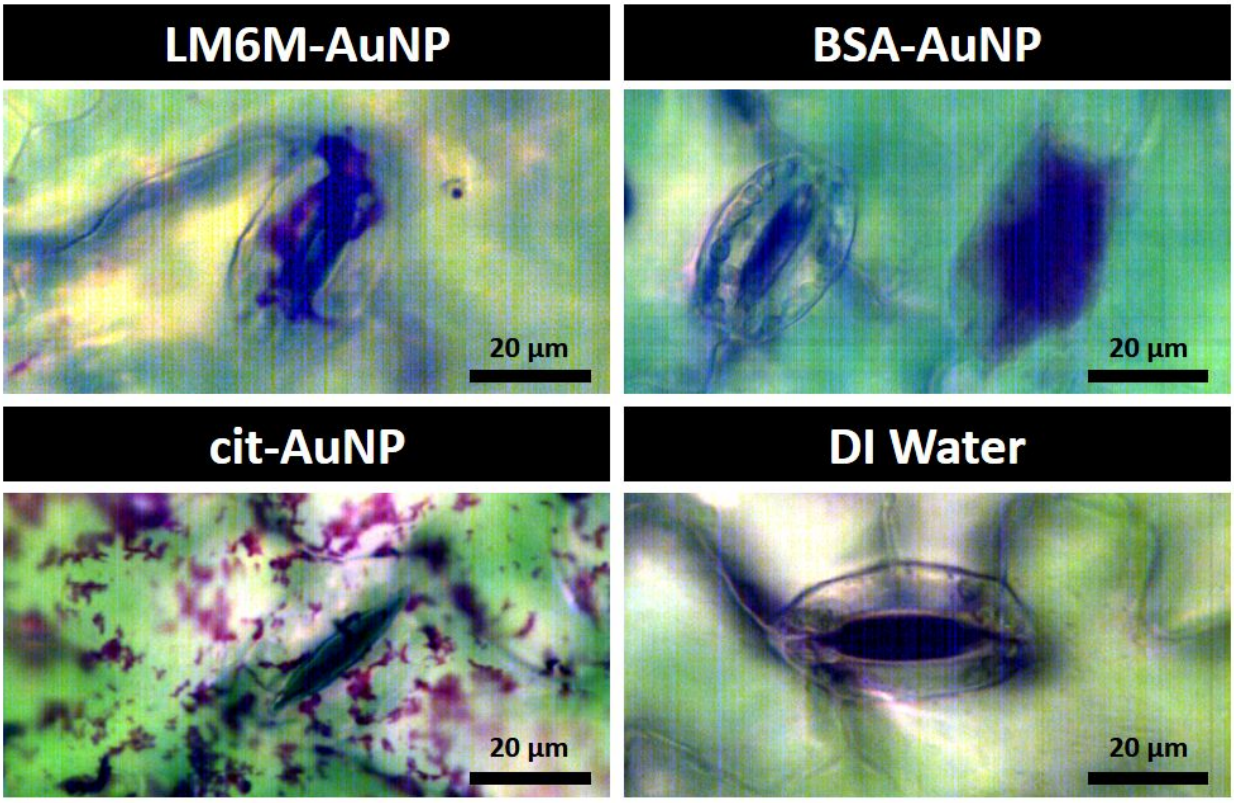

Fig. 2 Darkfield microscope images of the adaxial side of a *V. faba* leaf exposed via drop deposition to LM6M-AuNP, BSA-AuNP, cit-AuNP, and DI water and then rinsed for 2 min in a basal salt solution. Note the different NP accumulation (magenta/dark purple) depending on the NP coating around the stoma opening (LM6M), at the trichome head (BSA), or across the leaf surface (cit).

X-Ray Fluorescence Maps: XFM map showing Au distribution after exposure to LM6M-NP is shown in **Fig. 3**. As suggested by the darkfield microscope images, Au clearly accumulates around numerous stomata (stomata are indicated by red arrows), though there is also some additional adherence to other leaf features, possibly trichomes or other protein-rich features of the leaf where the cuticle is thin/absent.[27] Higher magnification light microscope image confirming the accumulation of Au with stomata is shown in **Fig. S4**. This suggests that the antibody coating was successfully able to deliver NPs to the stomata in a targeted manner.

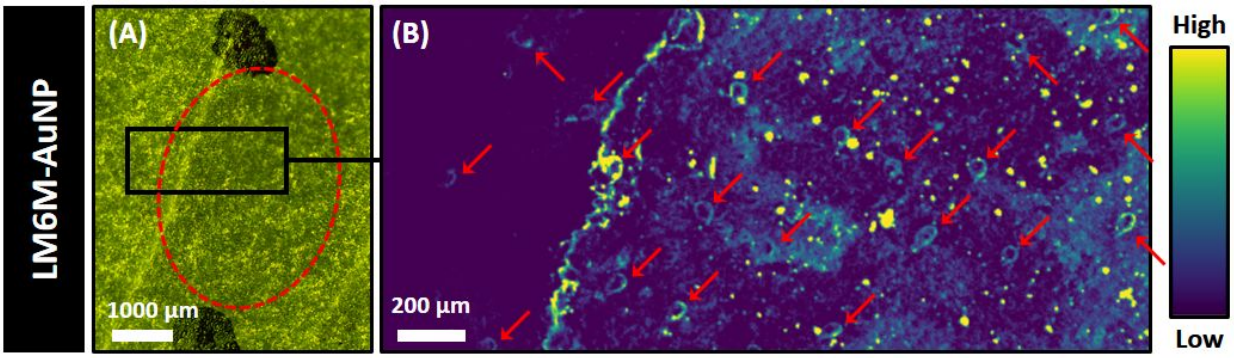

Fig. 3. Adaxial side of a *V. faba* leaf exposed via drop deposition to LM6M-AuNP, then rinsed for 2 min in a basal salt solution. (**A**) Light microscope image shows drop deposition zone between two black sharpie marks, as indicated by the red dashed oval, with the area scanned by XFM indicated by a black rectangle. (**B**) XFM map of Au distribution (see color scale to right), with stomata accumulation indicated by red arrows. Note: Au accumulation along the droplet outline is an artifact of air drying.

This image is in sharp contrast to that of the other two treatments (BSA-AuNP and cit-AuNP) shown in **Fig. 4**. *V. faba* stomata and trichomes, both of which contain potassium,[44] can be differentiated based on shape (**Fig 4, inset**). The cit-AuNP treatment in particular resulted in an even distribution of Au across the leaf surface. Larger light microscope image confirm the absence of Au on the stomata for the citrate in **Fig. S5**. Likewise, the BSA-AuNP treatment does not show accumulation of Au on the stomata. However, unlikely the cit-AuNP treatment, there is Au accumulation around some trichomes (see **Fig. S6** for evidence of trichome colocalization). Several papers have posited a hydrophilic uptake route of ionic species through the trichome

base.[44–47] Considering the BSA-AuNPs were significantly more electronegative, these particles could strongly partition to these more polar areas compared to the cit-AuNP or LM6M-AuNP. There are likely different hydrophilic functional groups around stomatal guard cells compared to the base of trichomes, though the exact differences would require further investigation. Despite using the same rinsing protocol for all exposure scenarios, rinsing was able to remove the BSA- and LM6M-AuNPs from the leaf surface better than for the cit-AuNP, which we hypothesize to be due to influence of NP size and charge on NP leaf adhesion. We have previously shown that larger 50 nm citrate-AuNPs can be more easily rinsed off the leaf surface than smaller 10 nm and 3 nm citrate-AuNPs.[10] Additionally, BSA-AuNPs have a higher magnitude negative zeta potential than cit- and LM6M-AuNPs, which could also explain the observed decrease in adhesion to the plant leaf surface through electrostatic repulsion, as hypothesized in previous studies.[10,18] Because the cit-AuNP are only electrostatically stabilized, they can aggregate irreversibly upon drying[42] and attach to the leaf cuticle more strongly than BSA- and LM6M-AuNPs that have protein coatings that provide steric repulsions, preventing aggregation and binding to the leaf cuticle.

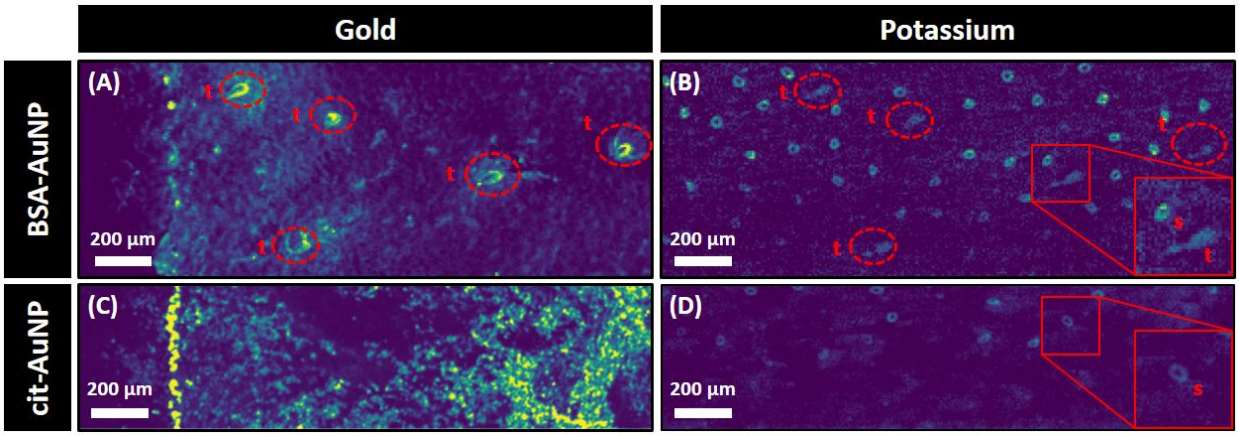

Fig. 4. XFM maps of (**A**, **C**) gold and (**B**, **D**) potassium distributions of the adaxial side of a *V. faba* leaf exposed via drop deposition to (**A**-**B**) BSA-AuNP or (**C**-**D**) cit-AuNP, then rinsed for 2 min in a basal salt solution. Majority of the hot spots on the potassium maps indicate stomata (*s*). trichome (*t*) accumulation in the BSA-AuNP exposure is highlighted with dashed red ovals. Inset

red boxes on the potassium maps (200 μm x 200 μm) show the differences in trichome and stomata shape. Note: Au accumulation along the droplet outline is an artifact of air drying

CONCLUSION

By coating NPs with an antibody with an affinity for α-1,5-arabinan, a chemical moiety found on stomatal guard cells, we demonstrated the successful targeted delivery of AuNPs to stomata on live *V. faba* leaves. In contrast, BSA-coated AuNPs had a specific affinity for trichomes. Though similar targeting has been used in nanomedicine, this is the first proof-of-concept study with plants. This is a step forward in testing the hypothesis that a targeted approach for pesticide application may be more efficient and effective than conventional non-targeted pesticide applications. Future studies can build off this work by using either antimicrobial NPs (e.g. CuO, Ag) or nanocarriers loaded with a pesticide to demonstrate higher efficacy at lower applied dose. Further work using the LM6M-AuNPs is also needed to test the antimicrobial efficacy of this stomata targeting, improve this stomata-specific affinity, and eliminate non-specific targeting as needed. Overall, massive innovations in pesticide and nutrient delivery systems in agriculture are needed to minimize environmental impacts from non-target effects of pesticides, and to minimize energy and water inputs resulting from inefficient use of fertilizers. The ability to provide delivery of pesticides to precise locations in the plant could revolutionize the way that agrochemicals are applied, providing greater efficacy, higher yields, and fewer off-target side effects (e.g. environmental degradation).

CONFLICTS OF INTEREST

There are no conflicts to declare.

ACKNOWLEDGEMENTS

This work is funded in part by the Dowd Fellowship from the College of Engineering at Carnegie Mellon University; the authors would like to thank Philip and Marsha Dowd for their financial support and encouragement. This material is also based upon work supported by the U.S. National Science Foundation (NSF) and the Environmental Protection Agency (EPA) under NSF Cooperative Agreement EF-1266252, Center for the Environmental Implications of NanoTechnology (CEINT) and Nano for Agriculturally Relevant Materials (NanoFARM) (CBET-1530563). Parts of this research used the XFM Beamline of the National Synchrotron Light Source II, a U.S. Department of Energy (DOE) Office of Science User Facility operated for the DOE Office of Science by Brookhaven National Laboratory under Contract No. DE-SC0012704 (Proposal #303572). This work was partially supported by Department of Energy-Geosciences under Grant No. DE-FG02-92ER14244. Cit-AuNPs were synthesized by Dr. Stella Marinakos at CEINT. The TEM images were completed at the Materials Characterization Facility at Carnegie Mellon University supported by grant MCF-677785.

REFERENCES

1 FAO, in *Proceedings of the Expert Meeting on How to Feed the Wold in 2050*, FAO Headquarters, Rome., 2009.

2 S. Savary, A. Ficke, J.-N. Aubertot and C. Hollier, *Food Secur.*, 2012, **4**, 519–537.

3 S. Savary, L. Willocquet, S. J. Pethybridge, P. Esker, N. McRoberts and A. Nelson, *Nat. Ecol. Evol.*, 2019, **3**, 430–439.

4 W. Zhang, *Global pesticide use: Profile, trend, cost / benefit and more*, 2018, vol. 8.

5 M. J. L. Castro, C. Ojeda and A. F. Cirelli, *Environ. Chem. Lett.*, 2014, **12**, 85–95.

6 G. V. Lowry, A. Avellan and L. M. Gilbertson, *Nat. Nanotechnol.*, 2019, **14**, 517–522.

7 S. M. Rodrigues, P. Demokritou, N. Dokoozlian, C. O. Hendren, B. Karn, M. S. Mauter, O. A. Sadik, M. Safarpour, J. M. Unrine, J. Viers, P. Welle, J. C. White, M. R. Wiesner and G. V. Lowry, *Environ. Sci. Nano*, 2017, **7**, 899–904.

8 P. Wang, E. Lombi, F.-J. Zhao and P. M. Kopittke, *Trends Plant Sci.*, 2016, **21**, 699–712.

9 R. Raliya, C. Franke, S. Chavalmane, R. Nair, N. Reed and P. Biswas, *Front. Plant Sci.*, , DOI:10.3389/fpls.2016.01288.

10 A. Avellan, J. Yun, Y. Zhang, E. Spielman-Sun, J. M. Unrine, J. Thieme, J. Li, E. Lombi, G. Bland and G. V. Lowry, *ACS Nano*, 2019, **13**, 5291–5305.

11 W. H. Elmer and J. C. White, *Environ. Sci. Nano*, 2016, **3**, 1072–1079.

12 K. Imada, S. Sakai, H. Kajihara, S. Tanaka and S. Ito, *Plant Pathol.*, 2016, **65**, 551–560.

13 J. Kurepa, T. Paunesku, S. Vogt, H. Arora, B. M. Rabatic, J. Lu, M. B. Wanzer, G. E. Woloschak and J. A. Smalle, *Nano Lett.*, 2010, **10**, 2296–2302.

14 Q. Dai, N. Bertleff-Zieschang, J. A. Braunger, M. Björnmalm, C. Cortez-Jugo and F. Caruso, *Adv. Healthc. Mater.*, 2017, **7**, 1700575.

15 D. J. McClements, *Compr. Rev. Food Sci. Food Saf.*, 2018, **17**, 200–219.

16 F. Torney, B. G. Trewyn, V. S.-Y. Lin and K. Wang, *Nat. Nanotechnol.*, 2007, **2**, 295–300.

17 A. Karny, A. Zinger, A. Kajal, J. Shainsky-Roitman and A. Schroeder, *Sci. Rep.*, 2018, **8**, 7589.

18 G. Liu, M. Yu, Y. Wang, J. Yao, H. Cui, J. Liang, Z. Zeng, B. Cui, C. Sun and X. Zhao, *RSC Adv.*, 2017, **7**, 11271–11280.

19 H. Wu, N. Tito and J. P. Giraldo, *ACS Nano*, 2017, **11**, 11283–11297.

20 J. P. Giraldo, M. P. Landry, S. M. Faltermeier, T. P. Mcnicholas, N. M. Iverson, A. A. Boghossian, N. F. Reuel, A. J. Hilmer, F. Sen, J. A. Brew and M. S. Strano, *Nat. Mater.*, 2014, **13**, 400–408.

21 S.-Y. Kwak, T. T. S. Lew, C. J. Sweeney, V. B. Koman, M. H. Wong, K. Bohmert-Tatarev, K. D. Snell, J. S. Seo, N.-H. Chua and M. S. Strano, *Nat. Nanotechnol.*, 2019, **14**, 447–455.

22 M. Melotto, W. Underwood and S. Y. He, *Annu. Rev. Phytopathol.*, 2008, **46**, 101–122.

23 M. Melotto, W. Underwood, J. Koczan, K. Nomura, S. Yang He and S. Y. He, *Cell*, 2006, **126**, 969–980.

24 G. W. Sundin, L. F. Castiblanco, X. Yuan, Q. Zeng and C. H. Yang, *Mol. Plant Pathol.*, 2016, **17**, 1506–1518.

25 R. C. Kirkwood, *Pestic. Sci.*, 1999, **55**, 69–77.

26 C. P. Bickford, *Funct. Plant Biol.*, 2016, **43**, 807–814.

27 S. M. Bird and J. E. Gray, *New Phytol.*, 2003, **157**, 9–23.

28 R. A. Burton, M. J. Gidley and G. B. Fincher, *Nat. Chem. Biol.*, 2010, **6**, 724–732.

29 J. Harholt, A. Suttangkakul and H. Vibe Scheller, *Plant Physiol.*, 2010, **153**, 384–395.

30 I. Shtein, Y. Shelef, Z. Marom, E. Zelinger, A. Schwartz, Z. A. Popper, B. Bar-On and S. Harpaz-Saad, *Ann. Bot.*, 2017, **119**, 1021–1033.

31 L. Jones, J. L. Milne, D. Ashford, M. C. McCann and S. J. McQueen-Mason, *Planta*, 2005, **221**, 255–264.

32 V. Cornuault, F. Buffetto, S. E. Marcus, M. C. Fabienne, G. M. Ralet and J. P. Knox, *bioRxiV*, 2017, 1–11.

33 Y. Verhertbruggen, S. E. Marcus, A. Haeger, R. Verhoef, H. A. Schols, B. V. McCleary, L. McKee, H. J. Gilbert and J. P. Knox, *Plant J.*, 2009, **59**, 413–425.

34 Y. Rossez, A. Holmes, H. Lodberg-Pedersen, L. Birse, J. Marshall, W. G. T. Willats, I. K. Toth and N. J. Holden, *J. Biol. Chem.*, 2014, **289**, 34349–34365.

35 D. H. Tsai, F. W. Delrio, A. M. Keene, K. M. Tyner, R. I. MacCuspie, T. J. Cho, M. R. Zachariah and V. A. Hackley, *Langmuir*, 2011, **27**, 2464–2477.

36 V. Silin, H. Weetall and D. J. Vanderah, *J. Colloid Interface Sci.*, 1997, **185**, 94–103.

37 J. Turkevich, P. C. Stevenson and J. Hillier, *Discuss. Faraday Soc.*, 1951, **11**, 55–75.

38 S. H. Brewer, W. R. Glomm, M. C. Johnson, M. K. Knag and S. Franzen, *Langmuir*, 2005, **21**, 9303–9307.

39 M. H. Jazayeri, H. Amani, A. A. Pourfatollah, H. Pazoki-Toroudi and B. Sedighimoghaddam, *Sens. Bio-Sensing Res.*, 2016, 9, 17–22.

40 J. P. Oliveira, A. R. Prado, W. J. Keijok, P. W. P. Antunes, E. R. Yapuchura and M. C. C. Guimarães, *Sci. Rep.*, 2019, **9**, 13859.

41 M. Newville, in *Journal of Physics: Conference Series*, IOP Publishing, 2013, vol. 430, p. 012007.

42 S. M. Louie, R. D. Tilton and G. V. Lowry, *Environ. Sci. Nano*, 2016, **3**, 283–310.

43 S. M. Louie, T. Phenrat, M. J. Small, R. D. Tilton and G. V. Lowry, *Langmuir*, 2012, **28**, 10334–10347.

44 T. K. Schlegel, J. Schönherr and L. Schreiber, *Planta*, 2005, **221**, 648–655.

45 L. Schreiber, *Ann. Bot.*, 2005, 95, 1069–1073.

46 C. Li, P. Wang, A. Van Der Ent, M. Cheng, H. Jiang, T. L. Read, E. Lombi, C. Tang, M. D. De Jonge, N. W. Menzies and P. M. Kopittke, *Ann. Bot.*, 2018, 1–12.

47 V. Fernández and T. Eichert, *CRC. Crit. Rev. Plant Sci.*, 2009, **28**, 36–68.

48 E. Spielman-Sun, A. Avellan, G. D. Bland, R. V Tappero, A. S. Acerbo, J. M. Unrine, J. P. Giraldo and G. V Lowry, *Environ. Sci. Nano*, 2019, **6**, 2508–2519.

TOC ART